The Role of O-antigen in the Response to Mechanical Stress of the E. coli Outer Membrane: Insights from Coarse-Grained MD simulations

Damien Jefferies[1], Jonathan Shearer[1] and Syma Khalid[1,*,†]

[1]School of Chemistry, University of Southampton, Southampton, SO17 1BJ, UK

*to whom correspondence should be addressed

† E-mail: S.Khalid@soton.ac.uk Phone: (023) 8059 4176

Abstract

Lipopolysaccharide (LPS) is an important component of the outer membrane of Gram-negative bacteria, contributing to the structural integrity of the bacterial cell wall and conferring resistance to chemical attack. The rough variant of LPS contains a conserved lipid A domain and complete core saccharide section, while the smooth variant additionally contains a terminal O-antigen chain. In the following, smooth LPS lipids are simulated in multicomponent membrane models using coarse-grained molecular dynamics. The simulations reveal that the lipid environment of smooth LPS lipids affects the orientation and clustering of their O-antigen chains. When the outer membrane leaflets contain smooth LPS lipids alone the O-antigen chains are packed tightly, leading to strong cohesive intermolecular interactions. When the outer leaflets incorporate interstitial phospholipids and rough LPS variants, the O-antigen chains are tilted and less tightly bound. The different packing of terminal O-antigen chains affects lipid mobility and the mechanical strength of the Gram-negative membrane models. Gram-negative membranes with outer leaflets of smooth LPS alone can withstand surface tensions (150 mNm^{-1}) that cause the membrane models with rough LPS lipids and comparable phospholipid bilayers to rupture much more readily.

Introduction

Gram-negative bacteria have complex cell envelope architecture: there is a thin layer of peptidoglycan that separates the inner cytoplasmic cell membrane from the asymmetric bacterial outer membrane.[1] The asymmetric bacterial outer membrane has an inner phospholipid leaflet, and an outer leaflet predominantly comprised of complex lipopolysaccharide (LPS) macromolecules, which confer resistance to chemical attack and contribute to the structural integrity of the cell wall. [2-4] LPS consists of lipid A, the hydrophobic moiety that anchors LPS to the outer leaflet of the outer membrane and a saccharide section, which varies in length and composition. When the LPS macromolecules contain terminal O-antigen chains they are rendered smooth, whereas the absence or reduction of O-chains makes LPS rough.[5]

Despite the prevalence of LPS molecules and their importance in the basic functioning of Gram-negative microbes, we currently lack a comprehensive understanding of many aspects of these lipids, particularly at the molecular level. In the following work, coarse-grained molecular dynamics simulations are performed to better understand the molecular level dynamics of smooth LPS. Simulations are performed with different Gram-negative outer membrane models: the membranes contain an inner phospholipid leaflet and outer leaflets comprised of smooth LPS lipids alone, smooth LPS lipids with rough variants of LPS, and LPS with small domains of palmitoyl-oleoyl-phosphatidylethanolamine (POPE) lipids. The bilayers are initially simulated at atmospheric pressure to understand the dynamics of tensionless membranes. The lateral pressure is then incrementally adjusted in a series of simulations to assess the response of smooth LPS lipids to mechanical stress.

The simulations reveal that the mobility and orientation of smooth LPS lipids depends sensitively on the lipids that surround them. When the outer leaflets incorporate combinations of smooth LPS, rough LPS, and interstitial phospholipids the terminal O-antigen chains adopt a tilted orientation (relative to the bilayer normal) that leads to interactions between distant polysaccharide

chains and subsequent clustering of separated smooth LPS lipids. The resulting leaflets of interstitial phospholipids, rough LPS, and clustered smooth LPS have moderate mechanical strength, withstanding surface tensions of no more than 100 mNm^{-1}. For leaflets comprised of smooth LPS lipids alone, the terminal O-antigen chains adopt lamellar packing that slows the LPS lipids and imparts significant mechanical strength, enabling the membranes to withstand surface tensions (150 mNm^{-1}) that cause comparable phospholipid bilayers to rupture.[6,7] To better understand the breakdown of the Gram-negative outer membrane, bilayer properties were monitored during the incremental increases in the lateral pressure magnitude. The increases in lateral pressure were associated with changes in O-antigen chain orientation and uniformity, bilayer thickness, area per lipid, and hydrophobic core permeability that led to the formation of disruptive transmembrane pores.

Comparable molecular dynamics simulations were recently performed to understand how mechanical stress is distributed in Gram-negative cell envelopes. However, the simulations made use of rough LPS, and so could not identify the important influence of O-antigen chains in increasing the outer membrane's ability to withstand high surface tension. [8] Similarly, experiments have been performed to assess the area compressibility modulus of different LPS variants[9,10] but the influence of O-antigen chains on membrane stability has not been systematically evaluated. When connections between LPS capping and mechanical stability have been made, the studies focused on the structural characteristics of bacterial biofilms[11] and provided no insight into the distribution of LPS lipids, the effect of interstitial phospholipids on membrane strength or the characteristics that are associated with the progressive degradation of Gram-negative membrane structure.

Methods

Simulations were performed with the GROMACS simulation package (version 5.1.2)[12] and the Martini force field (version 2.2).[13] Bilayers were assembled with the CHARMM-GUI Martini Bilayer Maker.[14,15] The web-based interface was used to select the relative abundances of lipids in the inner and outer leaflets that were hydrated with a solution containing sufficient Ca^{2+} ions to neutralize the LPS lipid A domain and core saccharide sugars, while the remaining system charge was neutralized through the use of monovalent Na^{+} ions. The slab of water and counterions was made sufficiently long ($\sim$ 10 nm above the LPS O-antigen chains) to minimize interactions between periodic images along the z-axis (parallel to the membrane normal). The inner bilayer leaflet contained POPE and POPG lipids in a 9:1 ratio for all membrane simulation systems, while the outer leaflets had the following compositions: smooth LPS (OANT), smooth LPS with POPE lipids in a 4:1 ratio (OANT_POPE), smooth LPS with rough LPS in a 1:1 ratio (MIXED), and smooth LPS with rough LPS and POPE in a 2:2:1 ratio (MIXED_POPE). The parameters for the rough LPS lipids, with R3 core sugars and type 1 lipid A, were previously determined through comparison with reference united-atom simulations of Gram-negative *E. coli* outer membrane models. Data from subsequent united-atom simulations of the *E. coli* O42 glycan polymer chain were used to expand this parameter set and enable the simulation of a smooth *E. coli* LPS lipid model, which includes lipid A, complete core saccharide section, and four repeat units of the O42 O-antigen chain. The parameterization is comparable to previous works on LPS macromolecules, but modifications have been made to bring coarse-grained simulations in line with our reference united-atom simulation data. The LPS models are made freely available within the CHARMM-GUI Martini Maker module, and a more comprehensive account of their parameterization is provided in our previous publications.[16,17]

The bilayers were equilibrated for 100 ns after initial energy minimization with the steepest decent algorithm. The temperature and pressure were controlled using the velocity-rescaling thermostat (at 313 K, with $\tau_{\mathrm{T}} = 1.0\ ps$) and the Parrinello-Rahman barostat (1 bar semi-isotropic pressure coupling, with $\tau_{\mathrm{P}} =$

5.0 ps).[18,19] All simulations were performed with an integration time step of 10 fs. Electrostatic interactions were modulated with the reaction field method using dielectric constants of 15 and infinity for charge screening in the short-range and long-range regimes, following the recommended simulation settings for coarse-grained Martini (version 2). The short-range cut-off distance for the electrostatic interactions was 1.2 nm. The Potential shift Verlet scheme was used to cut off the Lennard-Jones potential at long ranges.

Lateral pressures of increasing magnitude were applied to the equilibrated bilayers to assess their response to mechanical stress. The pressure coupling was semi-isotropic; the lateral pressure (P_L) was coupled separately from the pressure applied along the membrane normal (P_N). The lateral pressure magnitude was varied from -10 bar to -200 bar in independent simulations, while the pressure applied along the membrane normal was fixed at 1 bar. The strained bilayers were simulated for 20 μs each to allow sufficient time for the lipids to reach equilibrium configurations.

The order parameters were determined with the GROMACS *order* program. Lipid lateral diffusion was determined from mean square displacement curves that were computed for molecules in the membrane plane using the GROMACS *msd* tool. Radial distribution functions were determined with the GROMACS *rdf* tool. Distances were resolved with the GROMACS *mindist* tool. Angle distributions were calculated with the GROMACS *angle* program and number densities were computed with the GROMACS *densmap* tool. Area per lipid was determined through two-dimensional Voronoi tessellations of lipid phosphate groups. Systems were visualized with the Visual Molecular Dynamics package throughout.[20]

Results

Coarse-grained simulations were performed to assess the behavior of smooth *E. coli* LPS, with R3 core sugars, type 1 lipid A, and terminal O42 O-antigen chain, in different lipid environments. The smooth LPS macromolecules with complete

core sugar sequence and four repeat O-antigen chain units were inserted into lipid bilayers with POPE, POPG and rough LPS lipids using the CHARMM-GUI Martini Bilayer Builder. For each membrane, the lower leaflet contained POPE and POPG lipids in a 9:1 ratio (in line with the outer membrane of Gram-negative bacteria). The upper leaflets contained smooth LPS lipids alone (system OANT), smooth LPS with POPE lipids in a 4:1 ratio (system OANT_POPE), smooth LPS with rough LPS in a 1:1 ratio (system MIXED), or smooth LPS with rough LPS and POPE in a 2:2:1 ratio (system MIXED_POPE). The bilayers were solvated with a solution containing sufficient divalent Ca^{2+} ions to neutralize the charge of the lipid A and core saccharide LPS groups, while the remaining system charge was neutralized with monovalent Na^{+} ions. The systems were equilibrated for 100 ns and were then simulated for 2 μs at 313 K, enabling bilayer properties to converge (Figure S1).

The packing and dynamic interactions of the smooth LPS molecules depend sensitively on the type of lipids that surround them and on the availability of counterions that cross-link neighboring, negatively charged lipids. The smooth LPS lipids in system OANT have their acyl chains and O-antigen sugars distributed with a lamellar arrangement (Figure 1A-B). In contrast, the O-antigen sugars are tilted more substantially relative to the bilayer normal when the smooth LPS lipids are simulated in leaflets with neighboring rough LPS molecules and POPE lipids (Figure 1C-D). The O-antigen chains are oriented to maximize their intermolecular interactions with neighboring O-antigen chain polymers. In system OANT, O-antigen chain polymers maximize surface contact through their lamellar organization whereas O-antigen chains tilt to maximize surface contact in systems MIXED, MIXED_POPE, and to a lesser extent OANT_POPE due to the presence of interstitial phospholipids and rough LPS molecules.

In line with previous experimental and simulation studies, divalent cations help to reduce the unfavorable electrostatic interactions between neighboring LPS lipids by migrating to the LPS core saccharide sections and binding to exposed, negatively charged carboxylate and phosphate groups.[21-23] The pairwise radial

distribution functions for divalent Ca^{2+} ions around negatively charged phosphate and carboxylate groups (Figure S2) have first coordination shell values of ~ 75 at a distance comparable to the effective size of a coarse-grained Martini particle (σ = 0.47 nm). Comparable radial distribution functions are produced for simulations of cations around the phosphate groups of lipid A from Pseudomonas aeruginosa.[24] The divalent cations bridge neighboring phosphate and carboxylate groups, facilitating the aggregation of smooth and rough LPS lipids whereas monovalent Na^+ ions tend to form fewer interactions with exposed carboxylate and phosphate groups. The pairwise radial distribution functions for monovalent Na^+ ions around negatively charged phosphate and carboxylate groups have first coordination shell values of ~ 10 during the last 100 ns of simulation time. The divalent cations have favorable electrostatic interactions with the exposed carboxylate and phosphate groups and tend to preferentially coordinate the negatively charged sections of the LPS lipids.

The orientational mobility of lipid acyl chains is often quantified according to the equation $S = \frac{1}{2}\langle 3(\cos\theta)^2 - 1\rangle$, where θ is the time dependent angle between an acyl chain bond vector and the bilayer normal for a given snapshot in time.[25] Applying the equation to the LPS acyl chains in each membrane during the last 500 ns of simulation time, the average order parameters (with associated standard error estimates) are 0.20 ± 0.002, 0.20 ± 0.002, 0.24 ± 0.003, and 0.28 ± 0.003 for systems OANT, OANT_POPE, MIXED, and MIXED_POPE, respectively. Order parameters can also be calculated for the backbone chains of the O-antigen sugars to assess their order and orientation. The average order parameters for the O-antigen chain backbone beads in systems OANT and OANT_POPE are somewhat comparable to the acyl tail order parameters calculated for glycerophospholipid carbon tails in atomistic and coarse-grained simulations (Figure 1E).[26] The calculations demonstrate that the O-antigen sugars adopt approximate lamellar packing when they are embedded in leaflets of smooth LPS lipids, or leaflets of smooth LPS lipids with a small concentration of POPE lipids. In comparison, the O-antigen chain polymers have a more disordered arrangement in systems MIXED and MIXED_POPE, which contain a significant

proportion of rough LPS molecules and POPE lipids. The average order parameters for the backbone beads of the O-antigen polymer chains are 0.06 and 0.07 for systems MIXED and MIXED_POPE, respectively.

The angle between bond *O-anchor* (see Figure 1B), and the terminal O-antigen chain sugar was computed to better understand the orientation of the LPS O-antigen chains in each multicomponent membrane (Figure 1F). Calculated for the last 500 ns of simulation time, the angles and their associated standard deviations are: 101.2±1.1 (OANT), 75.2±1.0 (OANT_POPE), 86.5±1.9 (MIXED), and 68.7±2.8 (MIXED_POPE) degrees. Taken together, the data shows that the O-antigen chains are tilted most substantially (relative to the anchoring Lipid A and core sugar domains) in systems OANT_POPE, MIXED, and MIXED_POPE. Atomistic simulations of *E. coli* membrane models corroborate this conclusion: O-antigen chains are tilted more significantly (relative to membrane normal) when fewer comparable smooth LPS lipids surround them.[27] Likewise, when bilayers of smooth LPS from enterohemorrhagic *E. coli* (serogroup O91) were simulated with the CHARMM force field, the simulations revealed that the terminal O-antigen chains adopt approximately linear conformations, with the tilt angles between repeating glycan polymer units generally decreasing in magnitude further from the bilayer core, and generally being smaller than 25 degrees throughout.[28]

Overall, the relative order and orientation of LPS components depends on their environment: when smooth LPS lipids are bundled together, the neighboring O-antigen chains align along the bilayer normal, while the anchoring lipid tails splay outwards to reduce solvent accessible surface area in the bilayer core. The configuration produces relatively high order parameters for much of the O-antigen chains, and small angles between bond O-anchor and the terminal O-antigen chain sugars i.e. they closely align with the bilayer normal. When smooth LPS lipids are surrounded by rough variants of LPS and phospholipids, the O-antigen chains are unable to achieve comparable, lamellar alignment. Instead the O-antigen chains tilt and splay outwards to maximize their relative

intermolecular interactions across the bilayer surface. The terminal O-antigen chains display remarkable flexibility in the multicomponent membrane simulations, analogous to observations of smooth LPS lipids from atomistic molecular dynamics and statistical Monte Carlo simulations.[29,30] Importantly, there is limited interaction between the core LPS sugars and the terminal O-antigen chain polymers, which is supported by results from atomistic simulations of homogeneous, and mixed *E. coli* membrane models.[27,29]

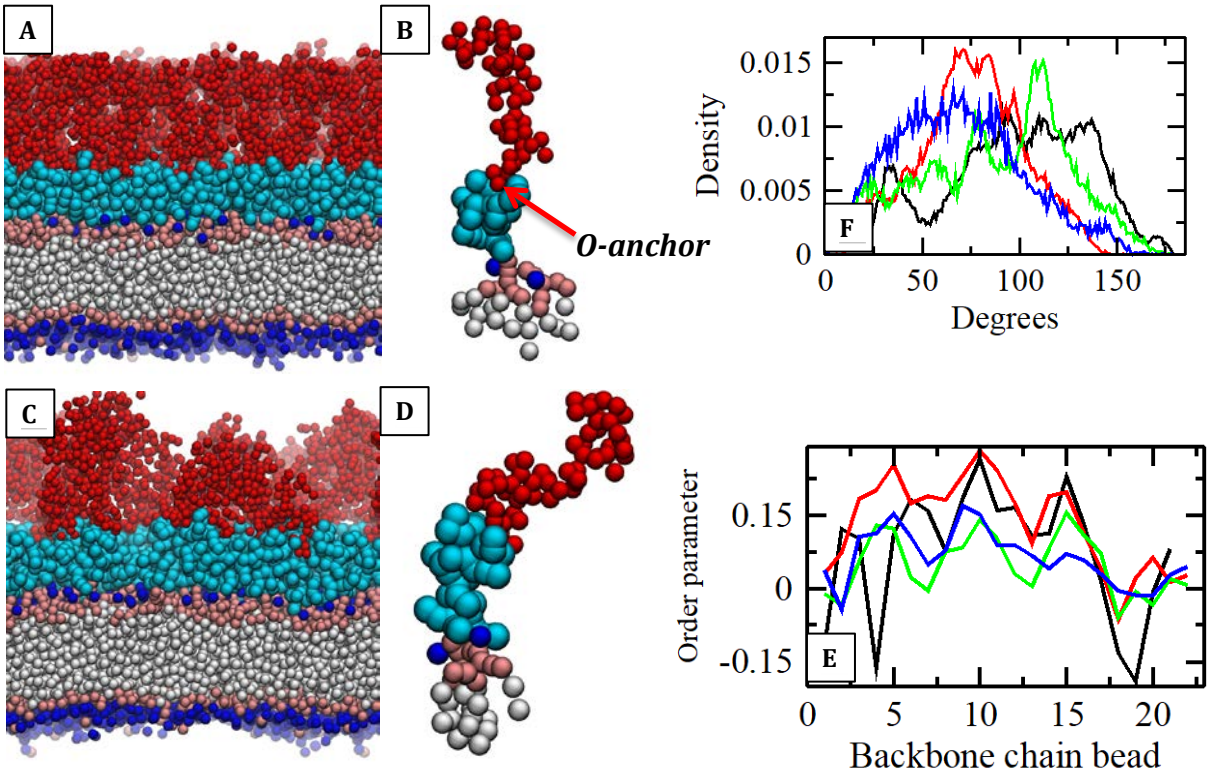

Figure 1. (A) Side view snapshot of system OANT, with (B) a single smooth LPS lipid extracted from the bilayer to show the orientation of the acyl chains and O-antigen chain sugars. The bond that anchors the O-antigen chain to the Lipid A and core sugar domains is termed '*O-anchor*' to make the discussion of LPS headgroup orientation more clear. (C) Side view snapshot of system MIXED_POPE, with (D) a single smooth LPS lipid extracted from the bilayer to show the orientation of the smooth LPS acyl chains and O-antigen chain sugars. The acyl tails are white, the phosphate groups are blue, the glycerol and glucosamine sugars are pink, core sugars are cyan, and terminal O-antigen chains are red, water molecules are omitted for clarity. (E) Average order parameters

calculated for the backbone chain beads of the O-antigen sugars in systems OANT (black), OANT_POPE (red), MIXED (green), and MIXED_POPE (blue). (F) Distribution for the angle formed by the *O-anchor* bond and the terminal O-antigen chain sugar in systems OANT (black), OANT_POPE (red), MIXED (green), and MIXED_POPE (blue).

The flexibility of the O-antigen chains in the MIXED and MIXED_POPE systems enables the O-antigen chains to interact across the lipid plane and thereby supports the clustering of smooth LPS headgroups. Figure 2A demonstrates this phenomenon for two smooth LPS lipids that were separated by ~ 4 nm at the start of the MIXED_POPE system simulation. Once the simulation is started, the O-antigen chains tilt relative to the bilayer normal and the smooth LPS lipids bind to each other after approximately 30 ns of simulation time (Figure 2B). The dimer then forms a larger aggregate as additional, neighboring smooth LPS lipids cluster together through the interactions of their terminal O-antigen chains (Figure 2C). Additional representative snapshots of the terminal O-antigen chains facilitating lipid clustering are included in the supplementary material (Figure S3).

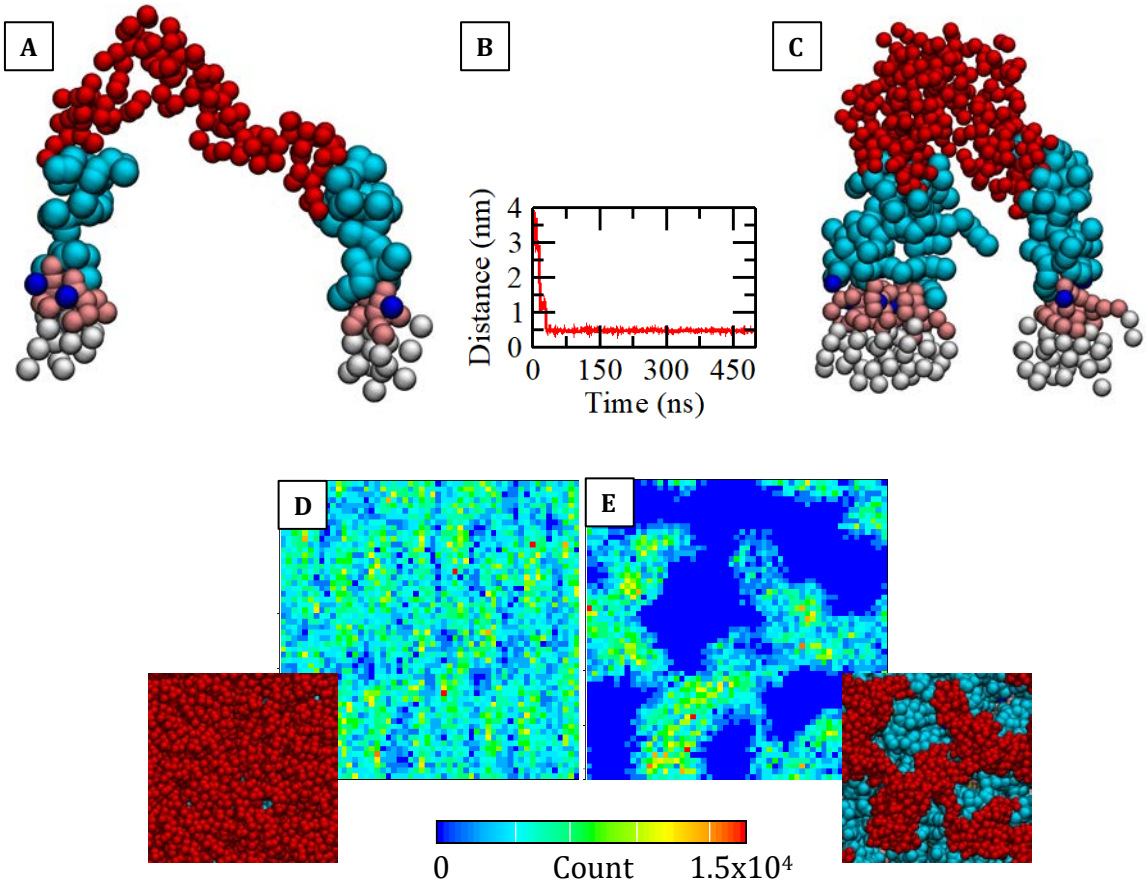

Figure 2. (A) Representative side view snapshot of two smooth LPS lipids clustering through the interactions of their tilted O-antigen chain sugars. (B) Time series for the distance between the two O-antigen chain sugars during the first 500 ns of simulation time. (C) Side view snapshot of the smooth LPS dimer forming a larger cluster of smooth LPS lipids. (D, E) Two-dimensional projection of O-antigen number density for systems OANT (D) and MIXED_POPE (E), the inset images show corresponding top view snapshots of each membrane.

The projection of O-antigen number density, which was computed by splitting the periodic box into a contiguous lattice with grid cells of size 0.2x0.2 nm, shows the overall effect of smooth LPS headgroup tilting and clustering. The O-antigen sugars have a relatively uniform distribution in system OANT (Figure 2D), but the O-antigen chains have a more asymmetric distribution for system MIXED_POPE (Figure 2E), system MIXED and system OANT_POPE. Moreover, in system OANT there are no intervening rough LPS and interstitial phospholipids to disrupt the cohesive interactions between neighboring O-antigen chains across the length of the membrane surface (Figure S4).

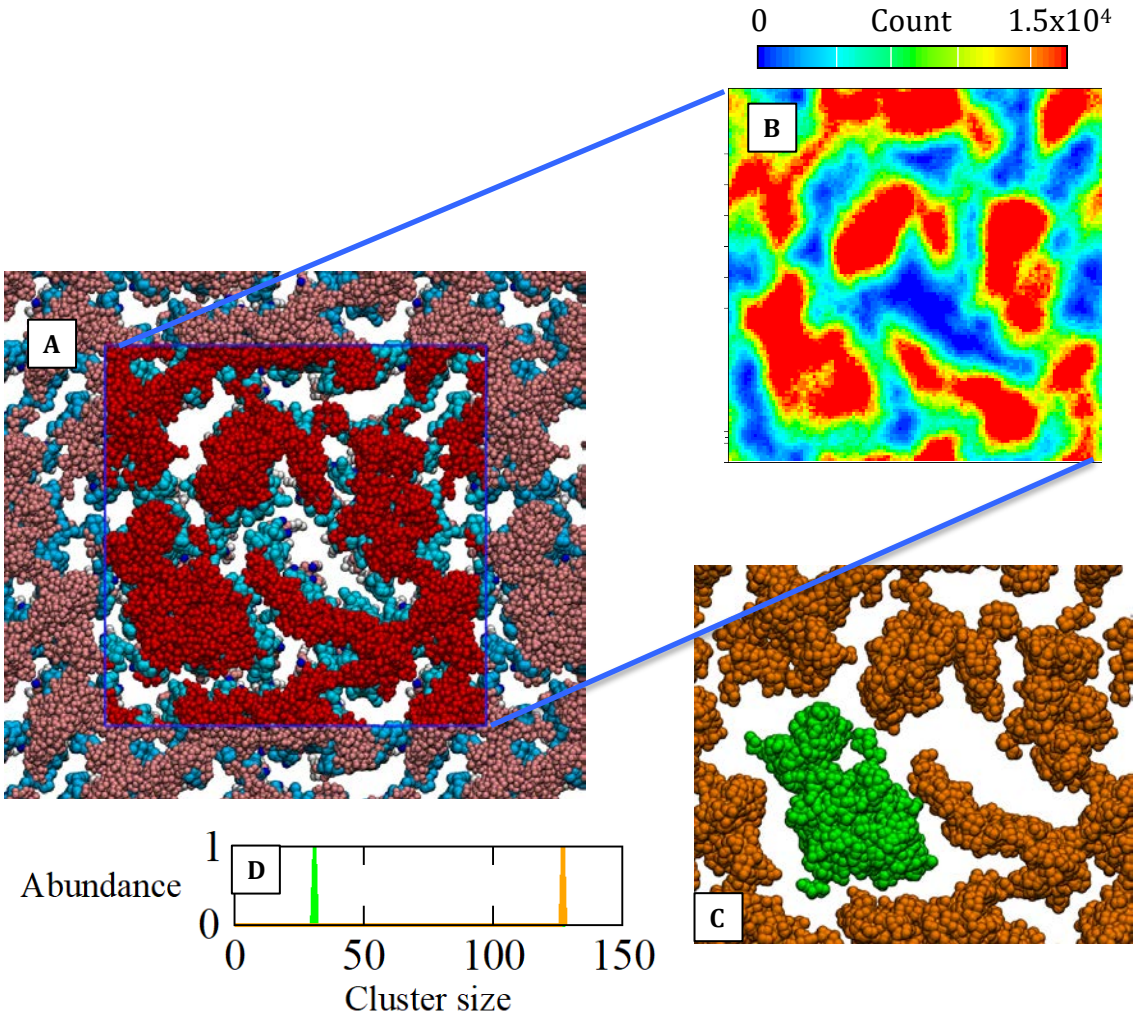

Figure 3. (A) Top view snapshot of a larger analogue of system OANT after 15 μs of simulation time. Water, ions, rough LPS, POPE and POPG molecules are excluded for clarity. The thin blue line represents the boundaries of the simulation cell and the periodic images are colored different shades of red and cyan to show lipid clustering. (B) Number density for the O-antigen chains of the smooth LPS lipids sampled over the last 100 ns of simulation time. (C) O-antigen aggregation is analyzed (using a 0.6 nm cutoff) and the two identified aggregates are colored green and orange. (D) The corresponding number of glycan polymer units in the identified O-antigen chain aggregates.

To better understand the clustering of smooth LPS, and in particular, the clustering of their terminal O-antigen chains, a larger analogue of system MIXED_POPE was simulated for 15 μs. The flexibility of the terminal O-antigen chains facilitates lipid demixing: the smooth LPS lipids segregate from neighboring rough LPS and POPE molecules to form clusters of smooth LPS lipids that span the length of the simulation cell (Figure 3A). This expansive network of smooth LPS is preserved during simulation time (Figure 3B), indicating that the clustering of smooth LPS, and the clustering of their O-antigens, is an energetically favorable process in Gram-negative outer membranes. Based on a 0.6 nm cut-off distance (GROMACS default), the smooth LPS lipids form a single, unbroken aggregate that spans the length of the simulation cell, while their terminal glycan polymers are divided between two distinct domains (Figure 3C-D). The interactions between neighboring O-antigen chains promote smooth LPS aggregation and lipid segregation, but the unusually strong cohesive interactions between neighboring LPS lipids, which supports strong correlated migration in molecular dynamics simulations[31,32] could be hindering further lipid demixing. In other words, segregation of LPS molecules from phospholipids is facile, but the partitioning of smooth LPS lipids and rough LPS lipids is less amenable to coarse-grained simulation.

The differences in lipid packing have important consequences for the structure and mobility of smooth LPS molecules. The average lateral diffusion rates were computed by sampling the mean square displacement curves, giving lateral

diffusion constants of 2.1 (OANT), 8.7 (OANT_POPE), 8.0 (MIXED), and 7.0 (MIXED_POPE) x10^{-8}cm^2/s. The lateral diffusion constants show that the mobility of smooth LPS lipids is significantly increased when rough LPS or glycerophospholipids surrounds them. Compared to previous publications, the computed lateral diffusion constants for smooth LPS lipids are intermediate to diffusion coefficients computed for rough units of LPS (5 x10^{-9}cm^2/s) and for their more dynamic B-band O-antigen chains (2 x10^{-7}cm^2/s).[29]

It is known that LPS lipids impart mechanical strength to the outer membrane of Gram-negative bacteria, making them resilient to attack from the external milieu. Given the differences in lipid organization in the simulation systems it is interesting to explore how embedded rough LPS molecules and glycerophospholipids affect the durability of Gram-negative outer membranes. Here, the lateral pressure component was incrementally adjusted to monitor the breakdown of the Gram-negative outer membrane models. The lateral pressure was set to -10 bar, -30 bar, -50 bar, -70 bar etc. in independent simulations that were simulated for 20 μs to ensure that lipid properties converged.

The surface tension-areal strain curve was computed for each multicomponent membrane to assess their relative mechanical strengths. The surface tension (γ) was calculated using the equation:

$$\gamma = L_z\,(P_N - P_L) \qquad (1)$$

Where L_z is the length of the simulation cell along the membrane normal, and P_N and P_L are defined in terms of the diagonal components of the pressure tensor (P_{xx}, P_{yy} and P_{zz}) according to $P_N = P_{zz}$ and $P_L = [P_{xx} + P_{yy}]/2$. The areal strain ($\varepsilon_{A)}$) was defined as:

$$\varepsilon_A = \frac{A_i}{A_0} - 1 \qquad (2)$$

where A_i and A_0 are the surface areas for bilayers simulated with lateral pressure P_L and in the tensionless states, respectively.

The surface tension-areal strain curves (Figure 4A) show unsurprisingly, that the membrane lipids increased their surface tension and minimized the exposure of their hydrophobic groups to water as the lateral pressure magnitude was incrementally increased. The data demonstrate that all membranes can withstand comparable lateral area expansion prior to formation of transmembrane pores that quickly cause membrane collapse. Utilizing displayed data, and data for bilayer rupture simulations, the area strain at the point of membrane rupture is 0.61-0.76, which is similar to critical areal strain values for phospholipid membranes in atomistic simulations.[6,33]

From the surface tension-areal strain curve, it is apparent that system OANT is characterized by higher surface tension (relative to system OANT_POPE, MIXED, and MIXED_POPE) indicating stronger attractive intermolecular interactions at the bilayer interface. Likewise, it is clear from the data that system OANT can withstand significantly increased surface tension prior to membrane collapse. The tight packing of smooth LPS O-antigen chains in system OANT, and their associated attractive intermolecular interactions, imparts appreciable mechanical strength that differs markedly from the comparable simulated membranes that contain interstitial phospholipids and rough LPS lipids in the LPS leaflet. The data demonstrates that system OANT can withstand a surface tension magnitude $\sim$ 60 mNm^{-1} larger than single component DPPC bilayers.[7] Additional comparisons with earlier, pioneering publications on membrane mechanical strength are limited given that (i) the phospholipid bilayers were generally simulated for less than 100 ns in early works[33,34] (ii) our coarse-grained simulations were run for a number of microseconds and (iii) that the speed of pore formation and bilayer breakdown depends on the magnitude of the applied pressure. [7] In other words, the use of coarse-grained resolution levels enabled the simulation of Gram-negative membrane models on a microsecond timescale and provided sufficient time for the spontaneous production of transmembrane pores that would otherwise have been missed if the production time were kept below 100 ns. Transmembrane pores can take

significantly longer than 100 ns to form in our molecular dynamics simulations and bilayers can seem, when compared with early publications, more liable to rupture given the significant differences in production time.

The structure of the bilayers changes significantly in response to increasing lateral pressure magnitude: there is a systematic increase in area per lipid (Figure 4B), a systematic decrease in membrane thickness (Figure 4C), and a general decrease in acyl tail order parameters (Figure 4D) with increasing lateral pressure magnitude. The outer membrane models successively thin and expand outwards with increasing lateral pressure magnitude, until pores appear in either the LPS or phospholipid leaflet that eventually leads to membrane breakdown.

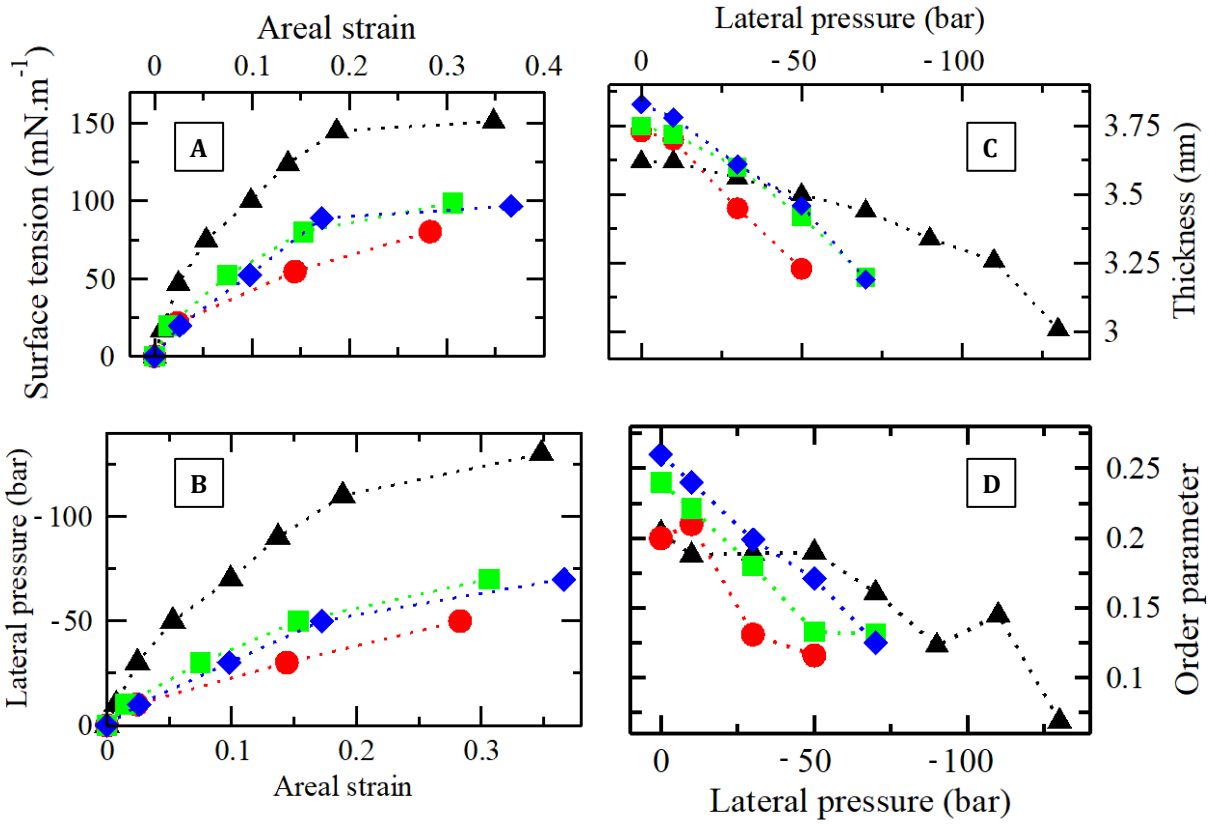

Figure 4. (A) Surface tension-areal strain curves. (B) Lateral pressure against areal strain (C) lateral pressure against membrane thickness and (D) lateral pressure against smooth LPS acyl tail order parameters. Data are shown for systems OANT (black), OANT_POPE (red), MIXED (green), and MIXED_POPE (blue). Data are excluded for lateral pressures that induced membrane rupture.

Given the unique stress-strain curve for system OANT, it seems appropriate to assess the changing orientation and interactions of constituent O-antigen chains during incremental increases in the lateral pressure magnitude and rationalize specific details that underpin the collapse and degradation of the Gram-negative outer membrane model. To this end, the order parameter has been computed for the O-antigen chain of smooth LPS lipids in system OANT for lateral pressure magnitudes that did not induce membrane rupture (Figure 5A). The data show an overall decrease in the order parameter of the backbone O-antigen chain beads, indicating a general reduction in the lamellar alignment of O-antigen chain polymers. This reduction in lamellar order of the O-antigen chains (relative to the bilayer normal) reduces the surface contact area between neighboring O-antigen chains and thereby reduces the number of cohesive intermolecular interactions between LPS headgroups that would otherwise contribute to membrane stability. This observation is supported by calculations of the changing angle formed by the *O-anchor* bond and terminal O-antigen chain sugars: the average O-antigen tilt angle was 9.5±1.5 degrees smaller for the OANT simulation with lateral pressure of -130 bar compared with the atmospheric pressure simulation. Moreover, two-dimensional particle number density maps reveal decreasing uniformity in O-antigen distribution as the lateral pressure magnitude was increased, contributing to weaker cohesive forces between neighboring smooth LPS lipids and their terminal O-antigen chains (Figure 5B-C).

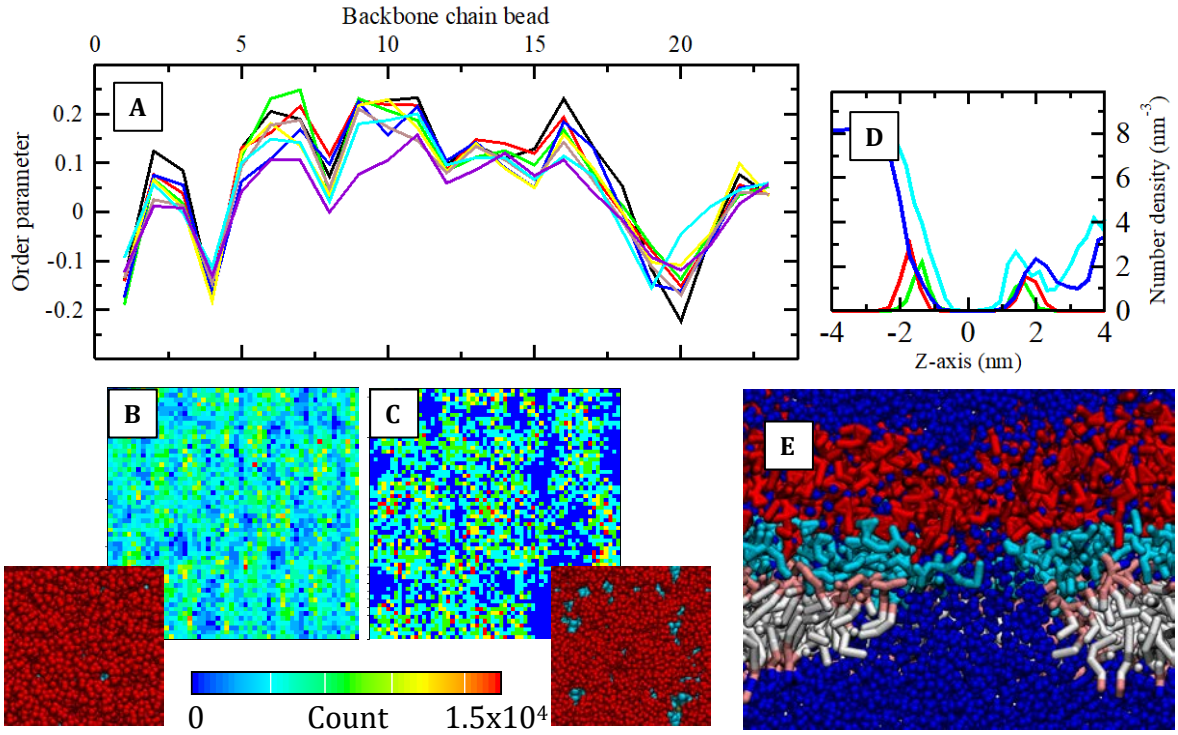

Figure 5. (A) Average order parameters for the backbone beads of O-antigen chain sugars in systems OANT simulated at atmospheric pressure (black) and lateral pressures of: -10 bar (red), -30 bar (green), -50 bar (blue), -70 bar (yellow), -90 bar (brown), -110 bar (cyan) and -130 bar (violet). (B, C) Two-dimensional O-antigen number density for system OANT at atmospheric pressure (B) and lateral pressure of -130 bar (C) during 10 ns of simulation time. The inset images show corresponding top view snapshots of each membrane. (D) Partial mass density plots for system OANT simulated at atmospheric pressure (red and blue lines) and with a lateral pressure of -130 bar (cyan and green lines). Partial mass densities for water are blue and cyan, and partial mass densities for phosphate groups are red and green. (E) Side view snapshot showing the spontaneous formation of a transmembrane pore in system OANT when it was simulated with a lateral pressure of -150 bar. Water particles are blue and smooth LPS lipids are colored as before.

Aside from changes in the structural parameters of system OANT in response to changing lateral pressure magnitudes, there was also a change in bilayer permeability. The calculation of phosphate group particle density shows that the hydrophobic core thinned in response to increasing lateral pressure magnitude (Figure 5D). Associated with this membrane thinning and lateral area expansion, there was an increase in the accessibility of the hydrophobic core. Water molecules successfully bypassed the interfacial phosphate groups and as a consequence, water flooded the extremities of the hydrophobic core. Overall, there was a breakdown of the interface between hydrophobic lipid tails and the encompassing hydrophilic solution. The distance between water beads on both sides of the membrane models was reduced and there was a smaller barrier for the formation of transmembrane water chains. Indeed, close monitoring of membrane collapse for simulations performed with lateral pressure magnitudes larger than -130 bar reveal that the breakdown of the bilayer structure was caused by the initial formation of transmembrane water chains that lead to the formation of transmembrane water channels (Figure 5E). After one pore was established, additional pores would appear in the bilayer and induce complete loss of lamellar lipid structure within 1 μs of simulation time.

Conclusion

LPS is a complex macromolecule that covers much of the Gram-negative cell surface,[35,4] and through strong cohesive interactions between individual LPS lipids, contributes to the structural integrity of the Gram-negative cell envelope. Smooth LPS is composed of three regions; (i) the conserved lipid A anchor, which embeds LPS molecules into the Gram-negative outer membrane; (ii) core oligosaccharides, and (iii) terminal O-antigen chain, which can be remarkably diverse among different bacteria.[2-4] In comparison, rough LPS is characterized by the absence or reduction of the O-antigen chain. [5]

Here, simulations were performed to understand the dynamic interactions of smooth LPS lipids in Gram-negative membrane models and their response to mechanical stress. The simulations revealed that the mobility and orientation of

smooth LPS lipids depends sensitively on the lipids that surround them. When rough LPS molecules and POPE lipids surround smooth LPS, the terminal O-antigen chains adopt a tilted orientation (relative to the bilayer normal). The skewed O-antigen chains are able to establish attractive intermolecular interactions leading to the clustering of neighboring O-antigen chain polymers. The leaflets of smooth LPS lipids alone and leaflets of smooth LPS lipids with POPE and rough LPS molecules differ in terms of mobility and mechanical strength. Gram-negative membrane models with one leaflet of smooth LPS lipids and one leaflet of phospholipids are relatively immobile and can withstand a surface tension (150 mNm^{-1}) that caused phospholipid membranes to rupture in previous simulation studies.[6-7,36] Whereas the incorporation of rough LPS lipids and interstitial phospholipids into the upper LPS leaflet increases molecular mobility, but drastically decreases the systems' tolerance for surface tension.

Analysis was performed to assess bilayer and LPS properties that precede the collapse of the Gram-negative outer membrane in response to large lateral pressure magnitudes. Incremental increases in lateral pressure magnitude were associated with increasing bilayer surface area and decreasing membrane thickness. Water molecules were able to more easily access the bilayer interior as the lateral pressure magnitude was increased, leading to reductions in bilayer stability. Moreover, LPS O-antigen chains became increasingly tilted and their distribution increasingly uneven as the lateral pressure magnitude was increased. Beyond a critical surface tension and a critical areal strain of 0.61-0.76 the membranes became perforated with transmembrane pores, leading to their complete degradation.

Although the simulations afford important insights into the durability of Gram-negative membranes and the stabilizing effects of interactions between their terminal O-antigen chains, it is important to appreciate the limitations of this coarse-grained simulation study. First, the low-resolution level of the LPS molecules limits the complexity of their conformational landscape and could preclude some of the diverse O-antigen chain conformations that are accessible

in atomistic simulations.[37] Second, the lack of explicit representation of divalent cations in Martini coarse-grained simulations can affect the configuration of individual LPS lipids and the interactions between them.[38-39,16]. Third, the unusually slow dynamics of LPS macromolecules[40-42] could preclude converged lipid configurations and prevent complete lipid segregation. LPS macromolecules display strong cohesive interactions between their anchoring lipid A domains,[31,43] which hinders the otherwise facile and relatively rapid mixing/demixing of comparable phospholipid bilayers.[44-46] Put another way, segregation of LPS molecules from phospholipids is facile, but the partitioning of smooth LPS lipids and rough LPS lipids is less amenable to conventional molecular dynamics. Fourth, the outer membrane of Gram-negative bacteria is more complex than our simplified bilayer models and can incorporate a wide range of different macromolecules e.g. outer membrane proteins[47-49] that can affect, at least locally, the physical properties of membrane lipids.[50,51]

Despite its limitations, this coarse-grained simulation study shows that the dynamics of smooth LPS lipids, and in particular the dynamics of their terminal O-antigen chains, are importantly influenced by the lipids that surround them. In turn, O-antigen chain polymers have distinct interactions with their neighbors that lead to differences in bilayer mechanical strength. Atomistic simulations of smooth LPS lipids, albeit with different LPS variants, corroborated conclusions that the membrane environment affects O-antigen chain interactions,[27,51] but the associated impact on bilayer strength has not been demonstrated, at least not empirically and systematically. The simulation study raises the question: are OANT system analogues assembled in vivo? The simulations of our most complex membrane models i.e. MIXED_POPE revealed that the formation of smooth LPS clusters is certainly favored, and further lipid demixing is feasible considering that there are strong cohesive interactions between LPS lipids that limit the segregation of smooth and rough variants of LPS on a microsecond timescale. Here, the presence of interstitial phospholipids accelerates the

assembly of LPS aggregates, but the coupling and decoupling of LPS macromolecules is likely to involve large energy barriers and occur on timescales not entirely amenable to conventional molecular dynamics. Experimentally it is found that LPS molecules display a strong preference for segregating in multicomponent membranes,[52] but their separation is a complex function of at least their size, shape and charge[53] and therefore, simple comparisons between our simulations and experimental data are limited. Simulations that incorporate outer membrane proteins have indicated that O-antigen chains preferentially tilt towards each other rather than the embedded bilayer proteins, suggesting their inclusion would not substantially affect data on bilayer strength and LPS clustering.[17]

The presented data help to develop a more comprehensive understanding of Gram-negative bacterial outer membranes, the interactions between their constituent LPS lipids, and their response to mechanical stress. The ability of bilayers to bear surface tension can importantly influence their ability to maintain their basic lamellar structure. The mechanical strength of bacterial membranes can for example, dictate their tolerance for osmotic pressures arising from differences in solute concentrations between the insides of cells and the external environment. Aside from offering insights into the preservation of cellular morphology in response to in vivo stressors e.g. turgor pressure, the data also helps clarify how synthetic outer membrane vesicles, which can be made void of transmembrane proteins and are therefore better mimics of our simulation systems, can be engineered to make them less prone to rupture or fuse, and thereby increase their shelf stability. The strength of lipopolysaccharide bilayers can evidently be modulated through LPS capping/O-antigen expression, providing a simple method to control the durability of outer membrane vesicles, which are increasingly being used as vaccine adjuvants and are garnering attention for their potential nanomedicinal applications.[54-56] Modulating the mechanical strength of comparable glycerophospholipid nanocarriers through the incorporation of amphiphilic block copolymers was

shown to not only enhance their shelf stability but also to reduce their toxicity, and increase the loading rates of drugs and drug cellular uptake.[57-59]

Going forward, the use of alternative simulation methods that can access longer timescales could help address the uncertainties regarding the conformation of smooth LPS clusters in the membrane models i.e. do our endpoint conformations represent converged lipid configurations? Simulations of alternative LPS variants could also reveal whether the relationship between O-antigen chain interactions and membrane mechanical strength is a trait of this LPS variant (*E. coli* LPS with O42 glycan polymer chain) alone, or if all terminal O-antigen chains regardless of shape, size and charge, can affect bilayer tolerance for surface tension.

Supporting Information

Four figures are provided. The figures demonstrate (i) bilayer convergence, (ii) the distribution of ions in the Gram-negative outer membrane models, (iii) snapshots of lipid clustering, and (iv) top view snapshots of different simulation systems.

Acknowledgement

The simulations were performed on the IRIDIS5 Compute Cluster at the University of Southampton and the ARCHER supercomputer through the HECBioSim Consortium supported by EPSRC (grant no. EP/R029407/1). J.S was supported by EPSRC through the TMCS CDT (grant no. EP/L015722/1).

References

1. Beveridge, T. J. Structures of Gram-Negative Cell Walls and Their Derived Membrane Vesicles. *J. Bacteriol.* **1999**, *181*, 4725-4733.
2. Rietschel, E.T.; Kirikae, T.; Schade, F. U.; Mamat, U.; Schmidt, G.; Loppnow, H.; Ulmer, A. J.; Zähringer, U.; Seydel, U.; Di Padova, F.; et al. Bacterial

Endotoxin: Molecular Relationships of Structure to Activity and Function *FASEB* **1994**, *8(2)*, 217–225.

3. Zhang, G.; Meredith, T. C.; Kahne, D. On the Essentiality of Lipopolysaccharide to Gram-Negative Bacteria, **2013**, *16(6),* 779–785.
4. Raetz C.R.; Whitfield C. Lipopolysaccharide Endotoxins *Annu. Rev. Biochem*. **2002**, *71*, 635–700.
5. Rittig, M. G.; Kaufmann, A.; Robins A.; Shaw, B.; Sprenger, H.; Gemsa, D.; Foulongne, V.; Rouot, B.; Dornand, J. Smooth and Rough Lipopolysaccharide Phenotypes of Brucella Induce Different Intracellular Trafficking and Cytokine/Chemokine Release in Human Monocytes *J. Leukoc. Biol*. **2003** *74(6)*, 1045–1055.
6. Zaki, A. M.; Carbone, P. How the Incorporation of Pluronic Block Copolymers Modulates the Response of Lipid Membranes to Mechanical Stress *Langmuir*, **2017**, *33(46),* 13284–13294.
7. Tomasini, M. D.; Rinaldi, C.; Tomassone, M. S. Molecular Dynamics Simulations of Rupture in Lipid Bilayers *Exp. Biol. Med.* **2010**, *235*: 181–188.
8. Hwang, H.; Paracini, N.; Parks, J. M.; Lakey, J. H. Distribution of Mechanical Stress in the *Escherichia coli* Cell Envelope *Biochim. Biophys. Acta* **2018** *1860(12)* 2566-2575.
9. Michel, J. P.; Wang, Y. X.; Kiesel, I.; Gerelli, Y.; Rosilio, V. Disruption of Asymmetric Lipid Bilayer Models Mimicking the Outer Membrane of Gram-Negative Bacteria by an Active Plasticin *Langmuir* **2017** *33(41)* 11028-11039.
10. Abraham, T.; Schooling, S. R.; Beveridge, T. J.; Katsaras, J. Monolayer Film Behavior of Lipopolysaccharide from Pseudomonas aeruginosa at the Air-Water Interface *Biomacromolecules* **2008** *9(10)* 2799-2804.
11. Lau, P. C. Y.; Lindhout, T.; Beveridge, T. J.; Dutcher, J. R.; Lam, J. S. Differential Lipopolysaccharide Core Capping Leads to Quantitative and Correlated Modifications of Mechanical and Structural Properties in Pseudomonas Aeruginosa Biofilms *J. Bacteriol.* **2009** *191(21)* 6618-6631.
12. Abraham, M. J.; Murtola, T.; Schulz, R.; Páll, S.; Smith, J. C.; Hess, B.; Lindahl, E. GROMACS: High Performance Molecular Simulations Through Multi-

Level Parallelism from Laptops to Supercomputers. *SoftwareX* **2015**, *1*, 19–25.

13. Marrink, S. J.; Risselada, H. J.; Yefimov, S.; Tieleman, D. P.; De Vries, A. H. The MARTINI Force Field: Coarse Grained Model for Biomolecular Simulations. *J. Phys. Chem. B* **2007,** *111(27),* 7812-7824.
14. Jo, S.; Kim, T.; Iyer, V.G.; Im, W. CHARMM-GUI: a Web-Based Graphical User Interface for CHARMM *J. Comput. Chem*. **2008** *29(11),* 1859-1865.
15. Hsu, P.; Bruininks, B.M.H; Jefferies, D.; de Souza, P.C.T; Lee, J.; Patel, D. S.; Marrink, S. J.; Qi, Y.; Khalid, S.; Im, W. CHARMM-GUI Martini Maker for Modeling and Simulation of Complex Bacterial Membranes with Lipopolysaccharides *J. Comput. Chem*. **2017,** *38(27),* 2354-2363.
16. Hsu, P.; Jefferies, D.; Khalid, S. Molecular Dynamics Simulations Predict the Pathways via Which Pristine Fullerenes Penetrate Bacterial Membranes *J. Phys. Chem. B*, **2016**, *120*(43), 11170–11179.
17. Shearer, J.; Jefferies, D.; Khalid, S. The Outer Membrane Proteins OmpA, FhuA, OmpF, EstA, BtuB and OmpX Have Unique Lipopolysaccharide Fingerprints *J. Chem. Theory Comput*. **2019,** (in press) DOI: 10.1021/acs.jctc.8b01059
18. Parrinello, M.; Rahman, A. Crystal Structure and Pair Potentials: A Molecular-Dynamics Study. *Phys. Rev. Lett*. **1980**, *45(14),* 1196.
19. Parrinello, M.; Rahman, A. Polymorphic Transitions in Single Crystlas: A New Molecular Dynamics Method. *J. Appl. Phys*. **1981** *52(12)*, 7182-7190.
20. Humphrey, W.; Dalke, A.; Schulten, K. VMD: Visual Molecular Dynamics J. *Mol. Graph. Model*. **1996**, *14(1)*, 33-38.
21. Schneck, E.; Schubert, T.; Konovalov, O.V.; Quinn, B. E.; Gutsmann, T.; Brandenburg, K.; Oliveira, R.G.; Pink, D.A.; Tanaka, M. Quantitative Determination of Ion Distributions in Bacterial Lipopolysaccharide Membranes by Grazing-Incidence X-ray Fluorescence *Proc. Natl. Acad. Sci. U. S. A.* **2010**, *107(20)*, 9147-9151.
22. Clifton, L.A.; Holt, S.A.; Hughes, A.V.; Daulton, E.L.; Arunmanee, W.; Heinrich, F.; Khalid, S.; Jefferies, D.; Charlton, T.R.; Webster, J.R.P et al. An Accurate in Vitro Model of the E. coli envelope *Angew. Chem. Int. Ed.* **2015**, *54(11)*, 11952-11955.

23. Oliveira, R.G.; Schneck, E.; Quinn, B.E.; Konovalov, O.V.; Brandenburg, K.; Gutsmann, T.; Gill, T.; Hanna, C.B.; Pink, D.A.; Tanaka, M. Crucial Roles of Charged Saccharide Moieties in Survival of Gram Negative Bacteria Against Protamine Revealed by Combination of Grazing Incidence X-ray Structural Characterizations and Monte Carlo Simulations *Phys. Rev. E* **2010**, *81(4),* 041901.
24. Li, A; Schertzer, J.W.; Yong, X. Molecular Dynamics Modeling of Pseudomonas Aeruginosa Outer Membranes *Phys. Chem. Chem. Phys.* **2018**, *20(36),* 23635-23648.
25. Vermeer, L. S.; de Groot, B. L.; Réat, V.; Milon, A.; Czaplicki, J. Acyl Chain Order Parameter Profiles in Phospholipid Bilayers: Computation from Molecular Dynamics Simulations and Comparison with ^{2}H NMR Experiments *Eur. Biophys. J.* **2007,** *36(8)*, 919–931.
26. Shearer, J.; Khalid, S. Communication Between the Leaflets of Asymmetric Membranes Revealed from Coarse-Grain Molecular Dynamics Simulations *Sci. Rep.* **2018**, *8*, 1805.
27. Wu, E.L.; Engström, O.; Jo S.; Stuhlsatz, D.; Yeom, M.S.; Klauda, J.B.; Widmalm, G.; Im, W. Molecular Dynamics and NMR Spectroscopy Studies of E. coli Lipopolysaccharide Structure and Dynamics *Biophys. J.* **2017***, 105(6), 1444-1455.*
28. Blasco, P.; Patel, D.S.; Engström, O.; Im, W.; Widmalm, G. Conformational Dynamics of the Lipopolysaccharide from Escherichia coli O91 Revealed by Nuclear Magnetic Resonance Spectroscopy and Molecular Simulations *Biochemistry* **2017**, *56(29),* 3826-3839.
29. Soares, T.A.; Straatsma, T.P.; Lins, R.D. Influence of the B-band O-antigen Chain in the Structure and Electrostatics of the Lipopolysaccharide Membrane of Pseudomonas Aeruginosa *J. Braz. Chem. Soc.* **2008***, 19(2),* 312-320.
30. Kastowsky, M.; Gutberlet, T.; Bradaczek, H. Molecular Modeling of the Three-Dimensional Structure and Conformational Flexibility of Bacterial Lipopolysaccharide *J. Bacteriol.* **1992***, 174(14),* 4798-4806*.*

31. Hsu, P.; Samsudin, F.; Shearer, J. It Is Complicated: Curvature, Diffusion, and Lipid Sorting within the Two Membranes of Escherichia coli *J. Phys. Chem. Lett*. **2017**, *8(22),* 5513-5518.
32. Jefferies, D.; Hsu, P.; Khalid, S. Through the Lipopolysaccharide Glass: a Potent Antimicrobial Peptide Induces Phase Changes in Membranes *Biochemistry* **2017,** *56(11),* 1672-1679.
33. Leontiadou, H.; Mark, A.E.; Marrink, S.J. Molecular Dynamics Simulations of Hydrophilic Pores in Lipids Bilayers *Biophys. J*. **2004**, *86(4),* 2156-2164.
34. Tieleman, P.; Leontiadou, H.; Mark, A.E.; Marrink, S.J. Simulation of Pore Formation in Lipid Bilayers by Mechanical Stress and Electric Fields *J. Am. Chem. Soc.* **2003**, *125(21),* 6382-6383.
35. Hancock, R.E.; Nikaido, H. Outer Membranes of Gram-Negative Bacteria. XIX. Isolation from Pseudomonas aeruginosa PAO1 and Use in Reconstitution and Definition of the Permeability Barrier *J. Bacteriol.* **1978**, *136(1),* 381-390.
36. Groot, R.D.; Rabone, K.L. Mesoscopic Simulation of Cell Membrane Damage, Morphology Change and Rupture by Nonionic Surfactants *Biophys. J.* **2001**, *81(2),* 725-736.
37. Galochkina, T.; Zlenko, D.; Nesterenko, A.; Kovalenko, I.; Strakhovskaya, M.; Averyanov, A.; Rubin, A. Conformational Dynamics of the Single Lipopolysaccharide O-antigen in Solution *ChemPhysChem* **2016**, *17(18),* 2839-2853.
38. Ma, H.; Irudayanathan, F.J.; Jiang, W.; Nangia, S. Simulating Gram-Negative Bacterial Outer Membrane: a Coarse Grain Model *J. Phys. Chem. B* **2015**, *199(46),* 14668-14682.
39. Van Oosten, B.; Harroun, T.A. A Martini Extension for Pseudomonas Aeruginosa PAO1 Lipopolysacchride *J. Mol. Graph. Model.* **2016**, *63*, 125-133.
40. Kirschner, K.N.; Lins, R.D.; Maass, A.; Soares, T.A. A Glycam-Based Force Field for Simulations of Lipopolysaccharide Membranes: Parameterization and Validation *J. Chem. Theory Comput*. **2012**, *8(11),* 4719-4731.

41. Pavlova, A.; Hwang, H.; Lundquist, K.; Balusek, C.; Gumbart, J.A. Living on the Edge: Simulations of Bacterial Outer-Membrane Proteins *BBA-Biomembranes* **2016**, *1858(7),* 1753-1759.
42. Soares, T.A.; Straatsma, T.P. Assessment of the Convergence of Molecular Dynamics Simulations of Lipopolysaccharide Membranes *Mol. Simul.* **2008**, *34(3),* 295-307.
43. Berglund, N.A.; Piggot, T.J.; Jefferies, D.; Sessions, R.B.; Bond, P.J.; Khalid, S. Interaction of the Antimicrobial Peptide Polymyxin B1 with Both Membranes of E. coli: a Molecular Dynamics Study *PLOS Comput. Biol.* **2015**, *11(4),* e1004180.
44. Carr, M.; MacPhee, C.E. Membrainy: a 'Smart', Unified Membrane Analysis Tool *Source Code Biol. Med*. **2015***, 10(1),* 1-10.
45. Qi, Y.; Ingólfsson, H.I.; Cheng, X.; Lee, J.; Marrink, S.J.; Im, W. CHARMM-GUI Martini Maker for Coarse-Grained Simulations with the Martini Force Field *J. Chem. Theory Comput*. **2015**, *11(9),* 4486-4494.
46. Barnoud, J.; Rossi, G.; Marrink, S.J.; Monticelli, L. Hydrophobic Compounds Reshape Membrane Domains *PLOS Comput. Biol*. **2014**, *10,* e1003873.
47. Faraldo-Gómez, J.D.; Smith, G.R.; Sansom, M.S.P. Molecular Dynamics Simulations of the Bacterial Outer Membrane Protein FhuA: a Comparative Study of the Ferrichrome-Free and Bound States *Biophys. J.* **2003**, *85(3),* 1406-1420.
48. Arunmanee, W.; Pathania, M.; Solovyona, A.S.; Le Brun, A.P.; Ridley, H.; Baslé, A.; van den Berg, B.; Lakey, J.H. Gram-Negative Trimeric Porins Have Specific LPS Binding Sites that are Essential for Porin Biogenesis *Proc. Natl. Acad. Sci. U. S. A.* **2016**, *113(34),* 5034-5043.
49. Straatsma, T.P.; Soares, T.A. Characterization of the Outer Membrane Protein OprF of Pseudomonas Aeruginosa in a Lipopolysaccharide Membrane by Computer Simulation Coarse-Grained MD Simulations of Membrane Protein-Bilayer Self-Assembly Proteins **2009**, *74(2),* 475-488.
50. Holdbrook, D.A.; Huber, R.G.; Piggot, T.J.; Bond, P.J.; Khalid S. Dynamics of Crowded Vesicles: Local and Global Responses to Membrane Composition *PLoS One* **2016**, *11(6):*e0156963.

51. Patel, D.S.; Re, S.; Wu, E.L.; Qi, Y.; Klebba, P.E.; Widmalm, G.; Yeom, M.S.; Sugita, Y.; Im, W. Dynamics and Interactions of OmpF and LPS: Influence on Pore Accessibility and Ion Permeability *Biophys. J.* **2016***, 110(4),* 930-938.
52. Kotra, L.P.; Golemi, D.; Amro, N. A.; Liu, G.; Mobashery, S. Dynamics of the Lipopolysaccharide Assembly on the Surface of *Escherichia coli J. Am. Chem. Soc*. **1999***, 121(38),* 8707-8711.
53. Kubiak, J.; Brewer, J.; Hansen, S.; Bagatolli, L. Lipid Lateral Organization on Giant Unilamellar Vesicles Containing Lipopolysaccharides *Biophys. J.* **2011**, 100(4), 978-986.
54. Tan, K.; Li, R.; Huang, X.; Liu, Q. Outer Membrane Vesicles: Current Status and Future Direction of These Novel Vaccine Adjuvants *Front. Microbiol.* **2018**, *9*:783.
55. Anand, D.; Chaudhuri, A. Bacterial Outer Membrane Vesicles: New insights and Applications *Mol. Membr. Biol.* **2016**, *33(6),* 125-137.
56. Bitto, N.J.; Chapman, R.; Pidot, S.; Costin, A.; Lo, C.; Choi, J.; D'Cruze, T.; Reynolds, E.C.; Dashper, S.G.; Turnbull, L.; et al. Bacterial Membrane Vesicles Transport Their DNA Cargo into Host Cells *Sci. Rep.* **2017**, *7*:7072.
57. Mandal, B.; Bhattacharjee, H.; Mittal, N.; Sah, H.; Balabathula, P.; Thoma, L.A.; Wood, G.C.; Core-Shell-Type Lipid-Polymer Hybrid Nanoparticles as a Drug Delivery Platform. *Nanomedicine* **2013**, *9(4)*, 474-491.
58. Chen, D.; Santore, M.M. Hybrid Copolymer-Phospholipid Vesicles: Phase Separation Resembling Mixed Phospholipid Lamellae, But With Mechanical Stability and Control. *Soft Matter* **2015**, *11(13)*, 2617-2626.
59. Zhang, R.X.; Cai, P.; Zhang, T.; Chen, K.; Li, J.; Cheng, J.; Pang, K.S.; Adissu, H.A.; Rauth, A.M.; Wu, X.Y. Polymer-Lipid Hybrid Nanoparticles Synchronize Pharmacokinetics of Co-Encapsulated Doxorubicin-Mitomycin C and Enable Their Spatiotemporal Co-Delivery and Local Bioavailability in Breast Tumor. *Nanomedicine* **2016**, *12(5)*, 1279-1290.

TOC graphic